Technical Report
V2 30–Jan–08

Parametrization of the exclusive π^+ electroproduction cross section at high energies

C. Weiss
Theory Center, Jefferson Lab, Newport News, VA 23606, USA

A simple analytic parametrization of the cross section for exclusive charged pion electroproduction $ep \to e' n \pi^+$ is described, valid at energies significantly above the resonance region, $W \gg 2\,\mathrm{GeV}$, and momentum transfers $Q^2 \ll W^2$ ("small x"). It is based on (a) a Reggeized Born term model for high–energy photoproduction, including π and ρ exchange; (b) vector dominance–like Q^2 dependence of electroproduction at $Q^2 < 1\,\mathrm{GeV}^2$; (c) extrapolation to higher Q^2 assuming QCD scaling behavior. The parametrization efficiently describes the photo– and electroproduction data from fixed–target experiments, and has the correct asymptotic behavior for extrapolation into the kinematics of collider experiments.

Contents

I. KINEMATIC VARIABLES AND CROSS SECTIONS

We consider exclusive electroproduction of charged pions (see Fig. 1),

$$e(l) + p(p) \;\to\; e'(l') + \pi^+(q') + n(p'), \tag{1}$$

where

$$q \;=\; l - l' \tag{2}$$

is the 4–momentum transfer to the hadronic system. The basic kinematic invariants are

$$\begin{aligned} s_{\mathrm{tot}} &= (l+p)^2 && ep \text{ squared CM energy} \\ Q^2 &= -q^2 && \text{photon virtuality} \\ W^2 &= (p+q)^2 && \gamma^* p \text{ squared CM energy} \\ t &= (p'-p)^2 && \text{invariant momentum transfer to nucleon} \end{aligned} \tag{3}$$

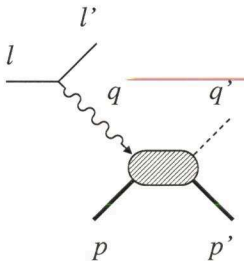

FIG. 1: Exclusive meson electroproduction.

Useful scaling variables are

$$\begin{aligned} x &= \frac{-q^2}{2(pq)} = \frac{Q^2}{W^2 - M_N^2 + Q^2} && \text{Bjorken variable,} \\ y &= \frac{(pq)}{(pl)} = \frac{Q^2}{x(s_{\mathrm{tot}} - M_N^2)} && \text{electron fractional energy loss.} \end{aligned} \tag{4}$$

The electroproduction differential cross section can be expressed in terms of the virtual photoabsorption cross section,

$$\begin{aligned} d\sigma(ep \to e'\pi^+ n) \;&=\; \Gamma\, dQ^2\, dW^2\, \frac{d\phi_e}{2\pi} \\ &\times\; d\sigma(\gamma^* p \to \pi^+ n), \end{aligned} \tag{5}$$

where ϕ_e is the azimuthal angle of the scattered electron with respect to the direction of the incident electron. The virtual photon flux is given by

$$\Gamma \;=\; \frac{\alpha(W^2 - M_N^2)}{2\pi(s_{\mathrm{tot}} - M_N^2)^2 Q^2}\, \frac{1}{1-\epsilon}, \tag{6}$$

where

$$\epsilon \;=\; \frac{1 - y - y^2 x^2 M_N^2/Q^2}{1 - y + y^2/2 + y^2 x^2 M_N^2/Q^2}. \tag{7}$$

is the photon polarization parameter. The virtual photoabsorption cross section is differential in the invariant momentum transfer to the nucleon, t, and the azimuthal angle of the produced pion with respect to the virtual photon direction, ϕ. It can be separated into contributions from amplitudes involving transverse and longitudinal photon polarization,

$$\begin{aligned} d\sigma(\gamma^* p \to \pi^+ n) \;&=\; \big[f_T + \epsilon\, f_L + \epsilon \cos 2\phi\, f_P \\ &+\; \sqrt{2\epsilon(1+\epsilon)} \cos\phi\, f_I\big]\; dt\, \frac{d\phi}{2\pi}, \end{aligned} \tag{8}$$

where we have omitted structures involving beam or target polarization. The functions f_T–f_I depend only on the invariants characterizing the virtual photon–nucleon subprocess and are independent of ϕ,

$$f_T \;=\; f_T(W^2, t, Q^2) \qquad \text{etc.} \tag{9}$$

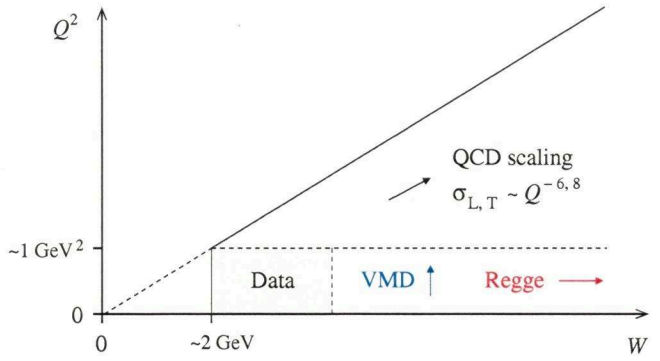

FIG. 2: Illustration of the W, Q^2–landscape of exclusive π^+ electroproduction and the dynamical models used in the parametrization of the cross section. The parametrization is constrained by data in the dark shaded region, and intended to be valid in the light shaded region.

In particular, f_T and f_L in Eq. (8) coincide with the usual ϕ–integrated differential cross section,

$$\frac{d\sigma_{T,L}}{dt} \equiv f_{T,L}(W^2, t, Q^2) \tag{10}$$

[the integration over $d\phi$ produces a factor 2π, which cancels the factor $1/(2\pi)$ in Eq. (8)]. In the following $d\sigma_{T,L}/dt$ will always be understood with this normalization. At $Q^2 = 0$, the virtual photon cross section reduces to the differential cross section for π^+ photoproduction,

$$d\sigma(\gamma p \to \pi^+ n) = [f_T + p \cos 2\phi \, f_P] \, dt \, \frac{d\phi}{2\pi}, \tag{11}$$

where $f_{T,P} \equiv f_{P,T}(W^2, t, Q^2 = 0)$, and $p \equiv \epsilon(Q^2 \to 0)$ is the degree of linear polarization of the photon beam.

II. CROSS SECTION PARAMETRIZATION

Our aim is to formulate a simple analytic parametrization of the cross section which efficiently describes the photo– and electroproduction data from fixed–target experiments, and has the correct asymptotic behavior for extrapolation into the kinematics of collider experiments. We do this by combining different dynamical models, valid in the different kinematic regions of interest (see Fig. 2):

(a) A Reggeized Born term model for the photoproduction cross section at energies $W > 2\,\text{GeV}$;

(b) Vector meson dominance– (VMD–) like Q^2 dependence in the low momentum transfer region $0 < Q^2 \lesssim 1\,\text{GeV}^2$;

(c) QCD scaling behavior of the cross sections in the region of momentum transfers $1\,\text{GeV}^2 < Q^2 \ll W^2$.

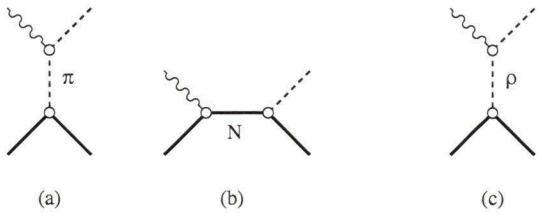

FIG. 3: Reggeized Born term model for high–energy π^+ photoproduction, $\gamma p \to \pi^+ n$ [1]. (a) π exchange; (b) Reggeized s–channel Born term included with π exchange; (c) ρ exchange.

A. Reggeized Born term model

For the photoproduction cross section we use the Reggeized Born term model of Ref. [1], which provides an efficient description of the existing data and implements the correct limiting behavior at high energies. It includes the the leading Regge trajectories in the π^+ production channel (π, ρ), see Fig. 3. The π exchange amplitude in this model includes the s–channel Born graph, whose destructive interference with the pion pole term turns the dip at $|t| < M_\pi^2$ (caused by the helicity flip in the pole term) into a maximum. The ρ exchange amplitude is treated as a pole term only. The Regge propagators assume degenerate trajectories and exhibit so–called non–sense wrong signature zeroes.

The basic objects of the model are the transition matrix elements of the EM current operator for the hadronic process,

$$\mathcal{J}_\mu(\lambda', \lambda) \equiv \langle n(\lambda')\pi^+ | \, J_\mu \, | p(\lambda) \rangle, \tag{12}$$

where $\lambda(\lambda')$ denote the helicity of the initial (final) nucleon. They are given by

$$\begin{aligned} \mathcal{J}_\mu^{(\pi)} &= \frac{i\sqrt{2} f_{\pi NN}}{M_\pi} \, \mathcal{P}^{(\pi)} \\ &\times 2M_N \, \bar{u}' \left[(\Delta - q')_\mu \, \gamma_5 \right. \\ &\left. - \frac{t - M_\pi^2}{W^2 - M_N^2} \gamma_5 (\hat{\Sigma} + M_N) \gamma_\mu \right] u. \end{aligned} \tag{13}$$

$$\begin{aligned} \mathcal{J}_\mu^{(\rho)} &= \frac{\sqrt{2} g_{\rho\pi\gamma} g_{\rho NN}}{M_\pi} \, \mathcal{P}^{(\rho)} \\ &\times \epsilon_{\mu\nu\rho\sigma} q_\nu \Delta_\rho \bar{u}' \left[\gamma_\sigma - \frac{\kappa_\rho}{2M_N} \sigma_{\sigma\tau} \Delta_\tau \right] u, \end{aligned} \tag{14}$$

with phenomenological coupling constants

$$f_{\pi NN} = 1.0, \tag{15}$$

$$g_{\rho\pi\gamma} = 0.103, \tag{16}$$

$$g_{\rho NN} = 3.4, \tag{17}$$

$$\kappa_\rho = 6.1. \tag{18}$$

Here Σ and Δ denote the total 4-momentum and the

momentum transfer of the photon–hadron process

$$\Sigma \equiv p+q = p'+q', \tag{19}$$
$$\Delta \equiv q-q' = p'-p, \tag{20}$$

with

$$\Sigma^2 = W^2, \tag{21}$$
$$\Delta^2 = t. \tag{22}$$

Furthermore, u and u' are the bispinors of the initial and final nucleon state, normalized according to $\bar{u}u = \bar{u}'u' = 2M_N$, $\hat{\Sigma} \equiv \Sigma^\nu \gamma_\nu$, and our convention for the Dirac matrices follows Ref. [2]. In Eqs. (13) and (14), $\mathcal{P}^{(\pi)}$ and $\mathcal{P}^{(\rho)}$ denote the scalar Regge propagators, which (assuming degenerate trajectories) are taken to be of the form

$$\mathcal{P}^{(\pi)} = \left(\frac{W^2}{W_0^2}\right)^{\alpha_\pi(t)} \exp[-i\pi\alpha_\pi(t)]\, \frac{\alpha'_\pi}{\alpha_\pi(t)}\, \Gamma[1-\alpha_\pi(t)], \tag{23}$$

$$\mathcal{P}^{(\rho)} = \left(\frac{W^2}{W_0^2}\right)^{\alpha_\rho(t)-1} \exp[-i\pi\alpha_\rho(t)]\, \alpha'_\rho\, \Gamma[1-\alpha_\rho(t)], \tag{24}$$

where $W_0^2 = 1\,\mathrm{GeV}^2$ is a scale parameter, and the trajectories are of the form

$$\alpha_\pi(t) = \alpha'_\pi(t-M_\pi^2) = \alpha_\pi(0) + \alpha'_\pi t, \tag{25}$$
$$\alpha'_\pi = 0.7\,\mathrm{GeV}^{-2}, \tag{26}$$
$$\alpha_\pi(0) = -\alpha'_\pi M_\pi^2 = -0.014; \tag{27}$$

and

$$\alpha_\rho(t) = \alpha_\rho(0) + \alpha'_\rho t, \tag{28}$$
$$\alpha_\rho(0) = 0.55, \tag{29}$$
$$\alpha'_\rho = 0.8\,\mathrm{GeV}^{-2}. \tag{30}$$

To calculate the cross section corresponding to the amplitudes Eqs. (13) and (14) one considers to introduce the hadronic tensor

$$W_{\mu\nu} \equiv \frac{1}{2}\sum_{\lambda',\lambda} \mathcal{J}_\mu(\lambda',\lambda)\, \mathcal{J}^*_\nu(\lambda',\lambda), \tag{31}$$

where we average (sum) over initial (final) nucleon helicities. The functions f_T–f_I describing the virtual photoabsorption cross sections, Eq. (8), are then obtained by expanding the hadronic tensor in a basis of virtual photon polarization vectors. Following standard convention, we choose coordinates such that the 3–momentum of the virtual photon points in the negative z direction, and the 3–momentum of produced pion has components in the xz plane. We introduce a set of polarization 4–vectors, $\epsilon^{(x)}, \epsilon^{(y)}$ and $\epsilon^{(z)}$, which are orthogonal to q, and together with q form an orthogonal basis,

$$q\epsilon^{(i)} = 0, \tag{32}$$
$$\epsilon^{(i)}\epsilon^{(j)} = 0 \qquad (i \neq j), \tag{33}$$
$$\epsilon^{(x)2}, \epsilon^{(y)2} = -1, \tag{34}$$
$$\epsilon^{(z)2} = 1. \tag{35}$$

The vectors $\epsilon^{(x)}$ and $\epsilon^{(y)}$ span the space of transverse photon polarizations, while $\epsilon^{(z)}$ corresponds to longitudinal polarization. In terms of

$$W^{(ij)} \equiv \epsilon_\mu^{(i)} \epsilon_\nu^{(j)} W_{\mu\nu}, \tag{36}$$

the photoabsorption cross sections are then given by

$$\left.\begin{matrix} f_T \\ f_L \end{matrix}\right\} = \frac{\alpha}{4(W^2-M_N^2)^2} \left\{ \begin{matrix} \frac{1}{2}\left(W^{(xx)} + W^{(yy)}\right), \\ W^{(zz)}. \end{matrix} \right. \tag{37}$$

In the high–energy limit,

$$W^2 \gg |t|, Q^2, M_N^2, M_\pi^2, \tag{38}$$

where the Regge model applies, the calculations can be carried out analytically, and one obtains:

$$\begin{aligned} \tfrac{1}{2}(W^{(xx)} + W^{(yy)}) &= \frac{2f_{\pi NN}^2}{M_\pi^2} && (2M_N)^2\,(M_\pi^4 + t^2) && \left|\mathcal{P}^{(\pi)}\right|^2 && (\pi \text{ exch.}) \\ &+ \frac{2g_{\rho\pi\gamma}^2 g_{\rho NN}^2}{M_\pi^2} && \left(1 - \frac{\kappa_\rho^2 t}{4M_N^2}\right) \frac{(-t)\,W^4}{2} && \left|\mathcal{P}^{(\rho)}\right|^2 && (\rho \text{ exch.}) \\ &+ \frac{2f_{\pi NN} g_{\rho\pi\gamma} g_{\rho NN}}{M_\pi^2} && \kappa_\rho t(t-M_\pi^2)\, W^2 && \mathrm{Re}\left[\mathcal{P}^{(\pi)}\mathcal{P}^{(\rho)*}\right] && (\pi\text{–}\rho \text{ interf.}) \end{aligned} \tag{39}$$

$$
\begin{aligned}
W^{(zz)} &= \frac{2f^2_{\pi NN}}{M^2_\pi} && (2M_N)^2\ (-t)Q^2 && \left|\mathcal{P}^{(\pi)}\right|^2 && (\pi \text{ exch.}) \\
&+ \frac{2g^2_{\rho\pi\gamma}g^2_{\rho NN}}{M^2_\pi} && (1+\kappa_\rho)^2 t^2 Q^2 && \left|\mathcal{P}^{(\rho)}\right|^2 && (\rho \text{ exch.}) \\
&+ \frac{2f_{\pi NN}g_{\rho\pi\gamma}g_{\rho NN}}{M^2_\pi} && (1+\kappa_\rho)t(t-M^2_\pi)\ \frac{8M^2_N Q^2}{W^2} && \mathrm{Re}\left[\mathcal{P}^{(\pi)}\mathcal{P}^{(\rho)*}\right] && (\pi\text{–}\rho \text{ interf.})
\end{aligned}
\tag{40}
$$

Here we have included the longitudinal components, which appear in electroproduction at $Q^2 > 0$ (see below). Several features of this result are worth noting:

- At $|t| \sim M^2_\pi$ the Reggeized pion propagator is close to the elementary propagator, $\mathcal{P}^{(\pi)} \approx 1/(t - M^2_\pi)$, and the transverse π exchange cross section behaves as

$$
\frac{d\sigma_T}{dt}(\pi \text{ exch.}) \sim \frac{t^2 + M^4_\pi}{(t - M^2_\pi)^2}, \tag{41}
$$

  exhibiting a peak at $t = 0$ of width $\sim M^2_\pi$. This feature is supported by the photoproduction data at energies up to $W^2 \sim 30\,\mathrm{GeV}^2$, indicating that the small–t cross section at these energies is indeed dominated by pion exchange (see Fig. 4) The ρ exchange cross section as well as the π–ρ interference cross section vanish for $t \to 0$.

- The W^2–dependence of the π and ρ exchange cross sections at small t is

$$
\frac{d\sigma_T}{dt}(\pi \text{ exch.}) \sim W^{2(2\alpha_\pi(0)-2)} \approx W^{-4}, \tag{42}
$$

$$
\frac{d\sigma_T}{dt}(\rho \text{ exch.}) \sim W^{2(2\alpha_\rho(0)-2)} \approx W^{-2}. \tag{43}
$$

  This implies that even at $|t| \sim M^2_\pi$ the ρ exchange cross section will eventually dominate at high energies, making the peak due to pion exchange disappear and qualitatively changing the t–dependence (see Fig. 4).

Overall, the model describes well the available high–energy photoproduction data (see Fig. 4).

B. Vector meson dominance

To model the Q^2 dependence in the soft high–energy regime, $Q^2 \lesssim 1\,\mathrm{GeV}^2$, we appeal to the notion of VMD (for a discussion of VMD in the context of charged pion production, see Refs. [4, 5]). In this approach the transverse electroproduction cross section is obtained from the photoproduction cross section as

$$
\frac{d\sigma_T}{dt}(Q^2) = \left(\frac{M^2_V}{M^2_V + Q^2}\right)^2 \frac{d\sigma_T}{dt}(Q^2 = 0), \tag{44}
$$

where $M_V \approx 0.77\,\mathrm{GeV}$ is the vector meson mass. In the pion pole term of the cross section, *cf.* Fig. 3a, such Q^2 dependence would be equivalent to a pion form factor of the usual monopole form, $F_\pi(Q^2) = 1/(1 + Q^2/M^2_V)$; however, here this dependence is assumed of the entire pion exchange cross section, including the s–channel Born term, Fig. 3b.

The longitudinal electroproduction cross section in the VMD approach is more model–dependent. Neglecting ρ–ω interference, and approximating

$$
\begin{aligned}
&\frac{1}{2}\left[\frac{d\sigma_T}{dt}(\gamma p \to \pi^+ n) + \frac{d\sigma_T}{dt}(\gamma n \to \pi^- p)\right] \\
&\approx \frac{d\sigma_T}{dt}(\gamma p \to \pi^+ n)
\end{aligned}
\tag{45}
$$

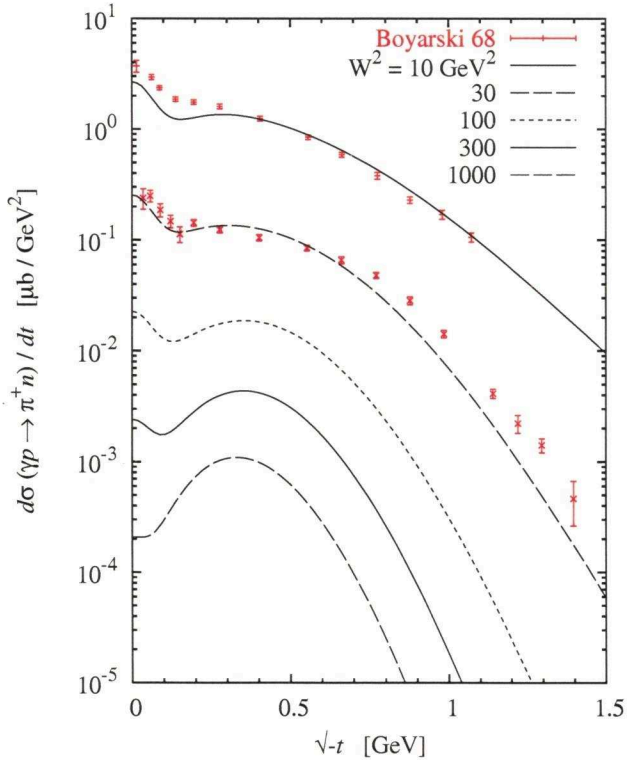

FIG. 4: The unpolarized π^+ photoproduction cross section $d\sigma_T/dt$ obtained from the Reggeized Born term model of Ref. [1], *cf.* Eq. (39), as a function of $\sqrt{-t}$. The data are from SLAC 1968 (Boyarski *et al.*) [3].

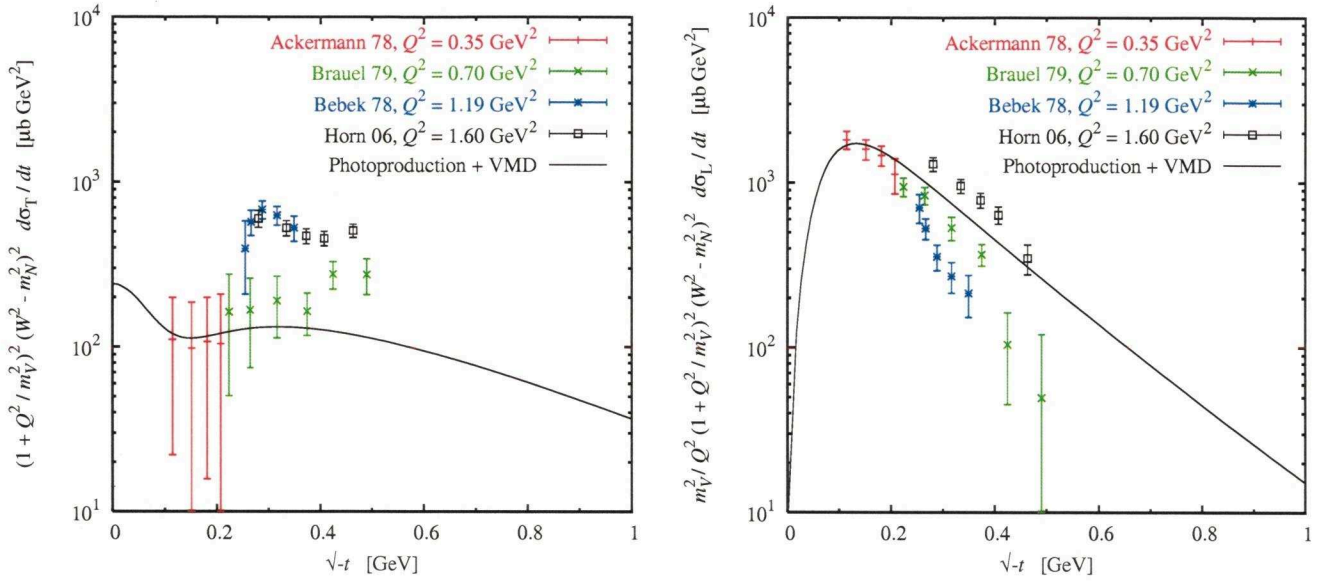

FIG. 5: Test of the Q^2–dependence predicted by VMD in π^+ electroproduction at $Q^2 \lesssim 1\,\mathrm{GeV}^2$. Plotted are the data for $d\sigma_T/dt$ (left panel) and $d\sigma_L/dt$ (right panel), rescaled such that the VMD–type Q^2–dependence, Eqs. (44) and (46) has been taken out; *i.e.*, if the data followed exactly the VMD prediction they should lie on a "universal" curve. The factor $(W^2 - M_N^2)^2$ has been scaled out to compensate for small differences in s between the data sets; the photoproduction data in this region of W show W–dependence $\propto (W^2 - M_N^2)^2$ (see Fig. 4). The data are from DESY 1978 (Ackermann *et al.*) [8], DESY 1979 (Brauel *et al.*) [9], Cornell 1976 (Bebek *et al.*) [10], and Jefferson Lab 2006 (Horn *et al.*) [11]. The curves show the predictions from the Reggeized Born term model, Eqs. (39) and (40).

we take

$$\frac{d\sigma_L}{dt}(Q^2) = \frac{Q^2}{M_V^2}\left(\frac{M_V^2}{M_V^2+Q^2}\right)^2 \frac{\rho_{zz}}{\frac{1}{2}(\rho_{xx}+\rho_{yy})} \times \frac{d\sigma_T}{dt}(Q^2=0), \tag{46}$$

where ρ_{zz} and $\frac{1}{2}(\rho_{xx}+\rho_{xx})$ are the spin density matrix elements describing ρ^0 production by charged pions. Thus, in the VMD approach the L/T ratio at $Q^2 \lesssim M_V^2$ is

$$\frac{d\sigma_L}{dt} \Big/ \left.\frac{d\sigma_T}{dt}\right|_{\mathrm{VMD}} = \frac{Q^2}{M_V^2}\,\frac{\rho_{zz}}{\frac{1}{2}(\rho_{xx}+\rho_{yy})}. \tag{47}$$

The ratio of ρ–meson density matrix elements has been measured in ρ^0 production by charged pions [6, 7]; see Fig. 1 of Ref. [4] for a summary plot. In principle, we could use a parametrization of these data for our purposes. It is simpler, however, to use the directly the result of the (Reggeized) Born term model, Eqs. (39) and (40), where the L/T ratio obtained from pion exchange (including the s–channel Born graph) is

$$\frac{d\sigma_L}{dt} \Big/ \left.\frac{d\sigma_T}{dt}\right|_{\text{Born } \pi \text{ exch.}} = \frac{(-t)Q^2}{M_\pi^4 + t^2}, \tag{48}$$

which would correspond to a ratio of ρ meson density matrix elements in Eq. (47) of

$$\frac{\rho_{zz}}{\frac{1}{2}(\rho_{xx}+\rho_{yy})} = \frac{(-t)M_V^2}{M_\pi^4 + t^2}. \tag{49}$$

It turns out that this function describes well the data from charged pion production at $|t| < 0.25\,\mathrm{GeV}^2$; see Fig. 1 of Ref. [4]. We will thus use the Born term model result (including ρ exchange) for $d\sigma_L/dt$, keeping in mind that it is effectively equivalent to VMD with the phenomenological rho meson density matrix elements, Eq. (47), at small t.

It is interesting to investigate how well the Q^2–dependence of low–Q^2 electroproduction data is described by VMD. In Fig. 5 we have plotted the data for $d\sigma_T/dt$ and $d\sigma_L/dt$ such that the VMD–type Q^2–dependence, Eqs. (44) and (46) has been taken out; *i.e.*, if the data followed exactly the VMD prediction they should lie on a "universal" curve. One sees that the data for $Q^2 < 1\,\mathrm{GeV}^2$ qualitatively support the VMD–like Q^2 dependence. The data at higher Q^2 show a systematic deviation, indicating the presence of a "harder" component in the cross section at $W \sim 2\,\mathrm{GeV}$ and high Q^2. The curves in Fig. 5 show the predictions from the Reggeized Born term model, Eqs. (39) and (40).

Figure 6 compares the results of the Reggeized Born term + VMD model directly with the low–Q^2 data from DESY 1978 (Ackermann *et al.*) [8] and DESY 1979 (Brauel *et al.*) [9], where VMD is applicable. One sees that the model reasonably well describes the data up to $|t| \sim 0.4\,\mathrm{GeV}^2$. The systematic deviations observed for larger t could be explained by assuming that the Born model no longer correctly describing the rho meson density matrix elements (in this region of t our model repre-

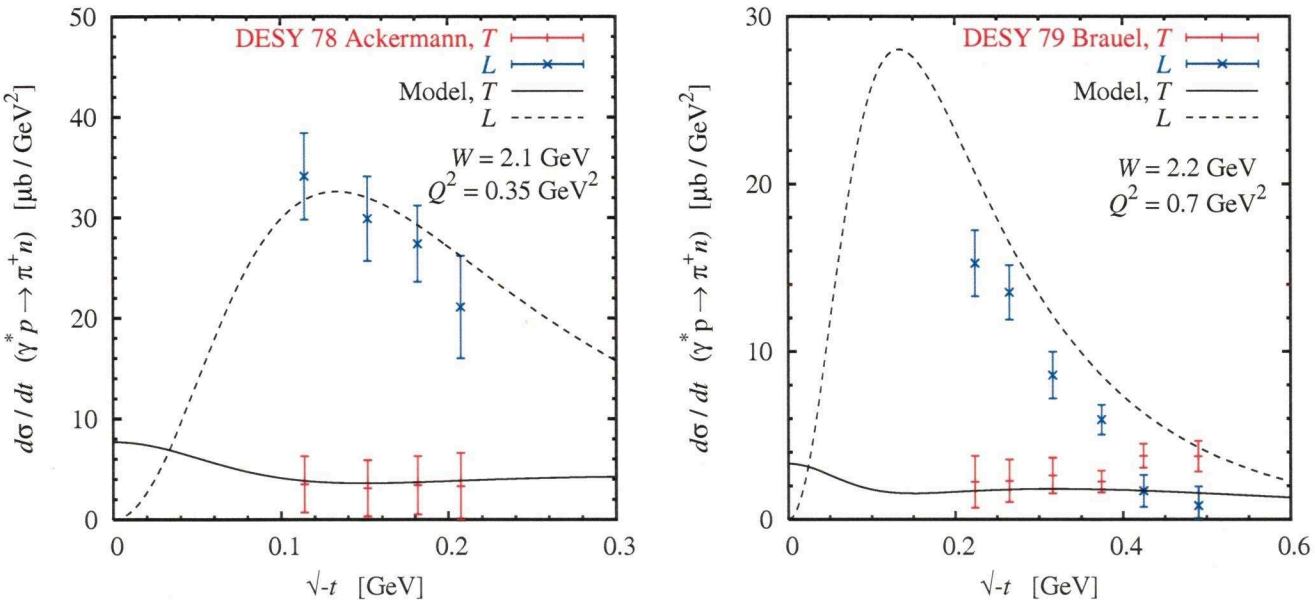

FIG. 6: Comparison of the predictions of the Reggeized Born term + VMD model with the low–Q^2 π^+ electroproduction data from DESY 1978 (Ackermann *et al.*) [8] (left panel), and DESY 1979 (Brauel *et al.*) [9] (right panel).

sents an extrapolation and the relation (49) is no longer supported by data); it does not necessarily imply a breakdown of VMD *per se*.

C. QCD scaling behavior

To model the cross section at larger values of Q^2, we invoke the scaling behavior implied by QCD factorization in the deep–inelastic limit ($Q^2, W^2 \to \infty$, with Q^2/W^2 fixed),

$$\frac{d\sigma_L}{dt} \sim Q^{-6}, \tag{50}$$

$$\frac{d\sigma_T}{dt} \sim Q^{-8}. \tag{51}$$

Assuming that the scaling behavior is valid starting from $Q^2 = Q_0^2 = 1\,\mathrm{GeV}^2$, we can extrapolate the cross section calculated in our Reggeized born term + VMD model into the high–Q^2 region. In practice, we calculate the cross section at a given $Q^2 > Q_0^2$ and given W^2 by determining the corresponding x–value,

$$x = \frac{Q^2}{W^2 - M_N^2 + Q^2}, \tag{52}$$

and extrapolating from Q_0^2 to Q^2 along the line of fixed x, using Eqs. (50) and (51). The W^2–value where this line hits $Q^2 = Q_0^2$ is given by

$$W_1^2 = \frac{1-x}{x} Q_0^2 + M_N^2, \tag{53}$$

and so we set

$$\frac{d\sigma_L}{dt}(W^2, Q^2) = \left(\frac{Q_0^2}{Q^2}\right)^3 \frac{d\sigma_L}{dt}(W_1^2, Q_0^2), \tag{54}$$

$$\frac{d\sigma_T}{dt}(W^2, Q^2) = \left(\frac{Q_0^2}{Q^2}\right)^4 \frac{d\sigma_T}{dt}(W_1^2, Q_0^2). \tag{55}$$

The prescription ensures that the cross sections have the correct asymptotic power behavior in the deep–inelastic regime; the coefficients of the leading powers are, of course, model–dependent.

The following points are worth noting:

- In the Reggeized Born term model with VMD, the π and ρ exchange cross sections for large values of W^2 and Q^2 scale as

$$\frac{d\sigma_L}{dt}(\pi \text{ exch.}) \sim Q^{-2}W^{-4} \sim Q^{-6}, \tag{56}$$

$$\frac{d\sigma_T}{dt}(\pi \text{ exch.}) \sim Q^{-4}W^{-4} \sim Q^{-8}, \tag{57}$$

$$\frac{d\sigma_L}{dt}(\rho \text{ exch.}) \sim Q^{-2}W^{-2} \sim Q^{-4}, \tag{58}$$

$$\frac{d\sigma_T}{dt}(\rho \text{ exch.}) \sim Q^{-4}W^{-2} \sim Q^{-6}, \tag{59}$$

  where the last column indicates the "would–be scaling" in the deep–inelastic region, $W^2 \sim Q^2$. One sees that in the case of π exchange the matching between the "soft" and "hard" Q^2–dependence is smooth; both have formally the same power behavior. In the case of ρ exchange the scaling behavior

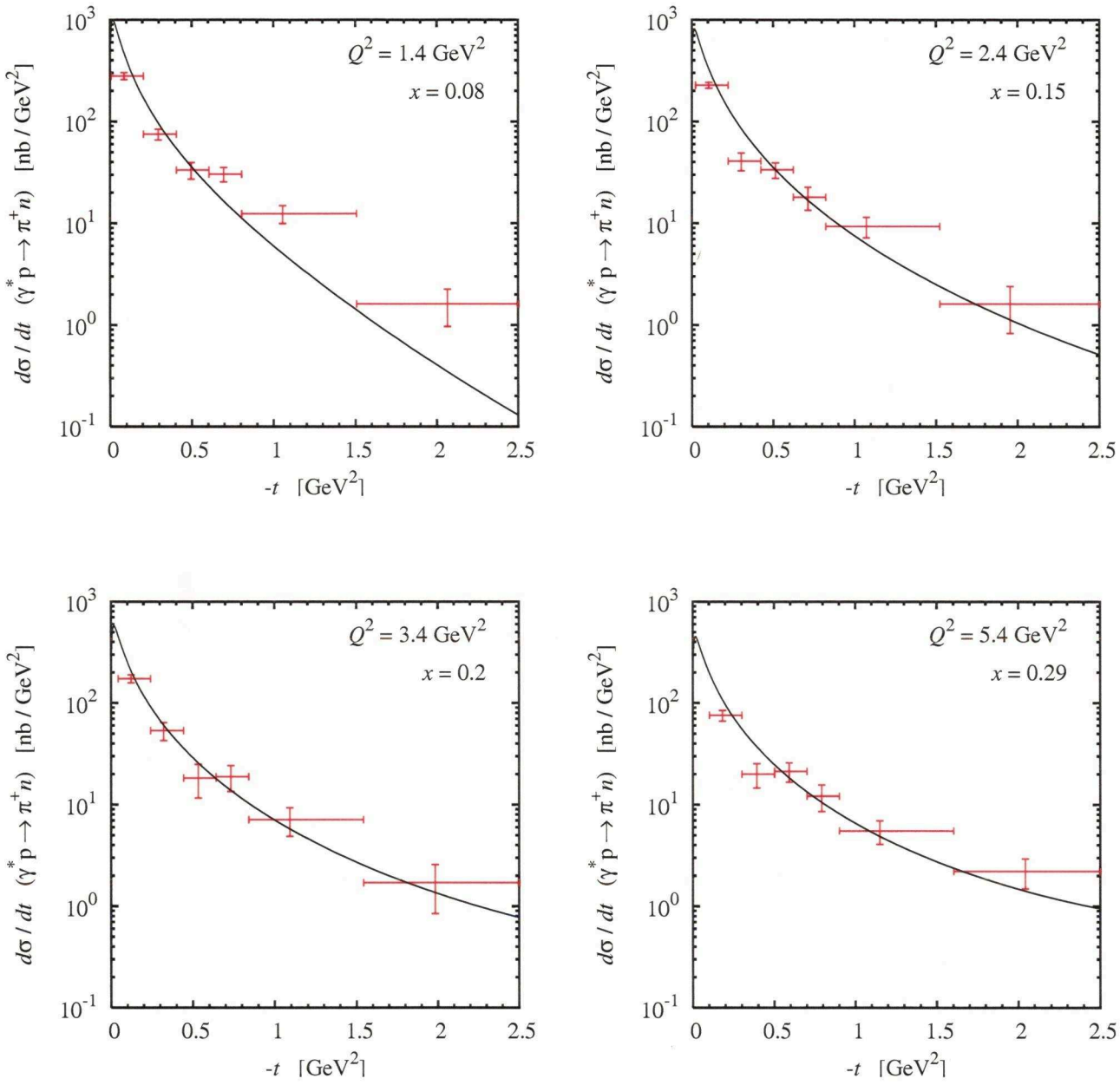

FIG. 7: Comparison of the extrapolated Reggeized Born term + VMD model with the data from DESY HERMES 2007 [12].

of the Born term model cross section is actually harder than the QCD scaling behavior; in this case the model must be understood as being limited to momentum transfers $Q^2 < Q_0^2$, and the extrapolation according to Eqs. (50) and (51) actually imposes a different dynamical behavior.

- In the Reggeized Born term model the t– and Q^2–dependence factorize [13]. Likewise, the extrapolation into the deep–inelastic region according to the QCD scaling behavior is done at fixed t and does not directly involve the t–dependence. Nevertheless, the extrapolation leads to an effective change of the t–dependence with Q^2 (at fixed W^2). This is because the t–dependence of the extrapolated cross section at Q^2 is the one implied by the Regge model at $W^2 = W_1^2$, and the value of W_1^2 decreases with Q^2. Thus, the t–slope of the cross section decreases with increasing Q^2. This behavior is analogous to the change of the t–distribution at fixed x with Q^2 induced by QCD evolution of the GPDs in the

deep–inelastic region.

Figure 7 compares the results of the full model (Reggeized Born term + VMD + QCD scaling) with the data from DESY HERMES 2007 (Airapetian *et al.*) [12]. One sees that the model reasonably describes the (L/T unseparated) data in the deep–inelastic region.

---

[1] M. Guidal, J. M. Laget and M. Vanderhaeghen, Nucl. Phys. A **627**, 645 (1997).

[2] V.B. Berestetskii, E.M. Lifshitz and L.P. Pitayevskii, in: Course of Theoretical Physics, Vol. IV: Relativistic Quantum Theory, Pergamon Press, Oxford, 1973.

[3] A. Boyarski *et al.*, Phys. Rev. Lett. **20**, 300 (1968).

[4] H. Fraas and D. Schildknecht, Phys. Lett. B **35**, 72 (1971); Phys. Lett. B **37**, 389 (1971).

[5] R. W. Manweiler and W. Schmidt, Phys. Rev. D **3**, 2752 (1971).

[6] D. Miller *et al.*, Phys. Rev. **153**, 1423 (1967).

[7] J. H. Scharenguivel *et al.*, Phys. Rev. Lett. **24**, 332 (1970).

[8] H. Ackermann *et al.*, Nucl. Phys. B **137**, 294 (1978).

[9] P. Brauel *et al.*, Z. Phys. C **3**, 101 (1979).

[10] C. J. Bebek *et al.*, Phys. Rev. Lett. **37**, 1326 (1976).

[11] T. Horn *et al.* [Jefferson Lab F(pi)-2 Collaboration], Phys. Rev. Lett. **97**, 192001 (2006) [arXiv:nucl-ex/0607005].

[12] A. Airapetian *et al.* [HERMES Collaboration], Phys. Lett. B **659**, 486 (2008) [arXiv:0707.0222 [hep-ex]].

[13] Note that we neglect $t_{\rm min}$ in Eqs. (39) and (40), consistently with the high–energy approximation $W^2 \gg Q^2, M_N^2, M_\pi^2$ in which the expressions were derived.

GH- 08.05.05

→ this model predicts ~2x higher $\frac{d\sigma}{dt}$ than Tanja's sig3000 over a wide range, from FπZ kinematics to $Q^2 = 10, W = 6$.
- so, I have arbitrarily divided this model by 2 when implementing it.

→ also, I note that in the $Q^2 = 10-25$ range, this model predicts a much lower $R = \sigma_T/\sigma_L$ ratio than sig3000 (which used VGL as input when doing the fits). So, I prefer to use Tanja's model as it is more conservative.